NANO LETTERS

2005
Vol. 5, No. 7
1237−1242

Size-Dependence of Surface Plasmon Resonance and Oxidation for Pd Nanocubes Synthesized via a Seed Etching Process

Yujie Xiong,[†] Jingyi Chen,[†] Benjamin Wiley,[‡] Younan Xia,[*,†] Yadong Yin,[§] and Zhi-Yuan Li[||]

Departments of Chemistry and Chemical Engineering, University of Washington, Seattle, Washington 98195, The Molecular Foundry, Lawrence Berkeley National Laboratory, Berkeley, California 94720, and Laboratory of Optical Physics, Institute of Physics, Chinese Academy of Sciences, Beijing 100080, People's Republic of China

Received May 11, 2005; Revised Manuscript Received May 24, 2005

ABSTRACT

Pd nanocubes between 8 and 50 nm in size were synthesized at the same concentration of Na_2PdCl_4 precursor by controlling the number of seeds formed in the nucleation stage. Increasing the concentration of $FeCl_3$, an oxidative etchant for Pd, reduced the number of seeds and led to formation of larger Pd nanocubes. The larger nanocubes exhibited surface plasmon resonance peaks in the visible region, the locations of which matched with the results of the discrete dipole approximation calculation. While the nanocubes of 25 and 50 nm in size oxidized in air to form Pd@PdO core−shell structures, the 8-nm nanocubes were stable in air for over 90 days.

Metal nanostructures have been of extensive interest for their widespread use in catalysis, photography, optics, electronics, optoelectronics, information storage, biological and chemical sensing, and surface-enhanced Raman scattering (SERS).[1−6] By tailoring the size and shape of metal nanoparticles, one can, in principle, tune their intrinsic properties for a range of applications. Shape-controlled synthesis has been achieved for many metals and alloys, such as Co, Ag, Au, Pt, and FePt, by growing seed particles in the presence of surfactants or polymers, through the thermal decomposition of organometallic compounds, with the mediation of biomolecules, or via the use of coordinating ligands.[7] In contrast, existing tools for control of particle growth such as variance of reaction temperature, precursor concentration, or surfactant concentration are often unable to adjust particle size in a broad range. As the number of seeds plays a large role in determining the size of a nanoparticle product, a more thorough study of the nucleation stage could directly provide a versatile tool for controlling the particle size.

Pd nanoparticles play an important role in many industrial applications.[8,9] They serve as the primary catalyst for low-temperature reduction of automobile pollutants[8] and for organic reactions, such as Suzuki, Heck, and Stille couplings.[9] In general, catalytic performance could be enhanced by controlling particle size. Another important property of Pd nanoparticles that remains largely unexplored is their surface plasmon resonance (SPR), which could lead to applications in colorimetric sensing, nanoscale waveguiding, enhancement of electromagnetic fields, and light transmission. Recently, the SPR of a Pd thin film was integrated into an optical sensor for hydrogen.[10] Using the discrete dipole approximation (DDA) method,[11] we found that 50-nm Pd nanocubes exhibit a resonant peak around 400 nm, while particles below 10 nm in size have no resonance between 300 and 1500 nm. Hence, control of nanoparticle size is critical for them to be useful in a potential application. To date, trigonal, hexagonal, cubooctahedral, and spherical Pd nanoparticles have been prepared by a variety of methods.[12] Although one can control their sizes by adjusting the amount of precursor, protective polymer, or surfactant, the controllable range is fairly narrow (1.7−7.0 nm).[12] Hence, it remains a grand challenge to tailor their size over a broad range.

Polyol reduction represents a powerful method for synthesizing metal nanoparticles.[13] We have recently improved this method for generating metal nanostructures with well-controlled shapes.[14] The essence of this synthesis is the reduction of a metal salt by ethylene glycol in the presence

* Author to whom correspondence should be addressed. E-mail: xia@chem.washington.edu.
[†] Department of Chemistry, University of Washington.
[‡] Department of Chemical Engineering, University of Washington.
[§] Lawrence Berkeley National Laboratory.
[||] Chinese Academy of Sciences.

10.1021/nl0508826 CCC: $30.25
Published on Web 06/03/2005

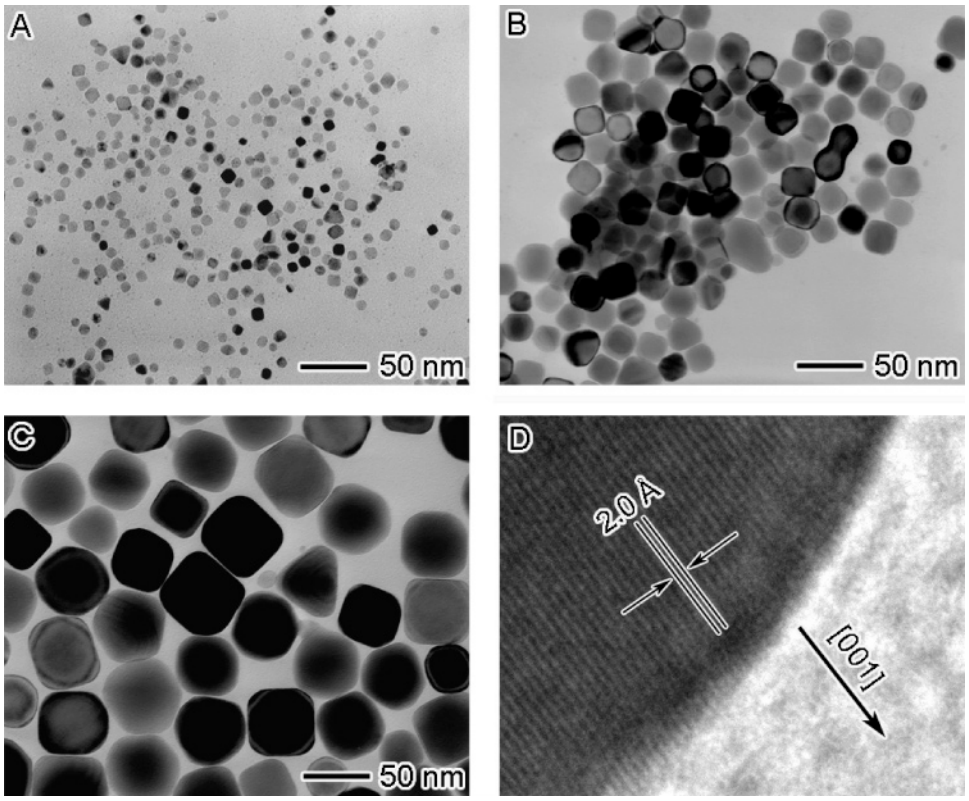

Figure 1. TEM images of Pd nanocubes with different sizes: (A) 8 nm, prepared without any $FeCl_3$; (B) 25 nm, prepared in the presence of 0.5 mM Fe $FeCl_3$; (C) 50 nm, prepared in the presence of 1.25 mM $FeCl_3$. The images in parts A−C are at the same magnification. (D) HRTEM image of one edge on a Pd nanocube (same sample as in part C).

of poly(vinyl pyrrolidone) (PVP). In the case of Pd, Pd atoms can be produced by reducing $PdCl_4^{2-}$ with ethylene glycol through the following reactions[15]

$$2HOCH_2CH_2OH \xrightarrow{\Delta} 2CH_3CHO + 2H_2O \quad (1)$$

$$PdCl_4^{2-} + 2CH_3CHO \rightarrow CH_3CO{-}OCCH_3 + Pd + 2H^+ + 4Cl^- \quad (2)$$

Most recently, we discovered that the oxidative etching of Pd by Cl^-/O_2 could selectively remove multiple twinned particles involved in the polyol synthesis of Pd nanoparticles.[15] Such an etching process resulted in high yields of monodispersed, single-crystal cubooctahedra of ~8 nm in dimension. Since the amount of O_2 dissolved in ethylene glycol and adsorbed on the surface of Pd particles is limited and hard to control, we also explored other oxidants that could be quantitatively added to the reaction solution. Fe^{III} is a well-established wet etchant for noble metals.[16] As we have demonstrated, addition of Fe^{III} to the polyol reduction of H_2PtCl_6 could oxidize Pt atoms back to Pt^{II} and slow the growth rate of Pt seeds so that preferential addition of atoms along the ⟨111⟩ axis led to the formation of uniform Pt nanowires.[14b] In the present work, we obtained Pd nanocubes with sizes >20 nm by coupling polyol reduction with oxidative etching by Fe^{III}.[17] As suggested by the standard electrical potentials of the redox reactions involved in this system, Fe^{III} could oxidize atomic Pd (e.g., seeds) back to Pd^{II} in the solution and compete with reaction 2[18]

$$Fe^{3+} + e^- \rightarrow Fe^{2+} \quad E^0 = 0.77 \text{ V}$$

$$PdCl_4^{2-} + 2e^- \rightarrow Pd + 4Cl^- \quad E^0 = 0.59 \text{ V}$$

The oxidative etching of Pd seeds by Fe^{III} could reduce the number of seeds formed in the nucleation step. At the same concentration of Pd precursor, a decrease in the number of seeds resulted in the production of nanocubes with larger sizes.

Figure 1A shows TEM images of samples taken from a typical synthesis, in which Na_2PdCl_4 was reduced by ethylene glycol in the presence of PVP without addition of Fe^{III}. The sample mainly contained truncated nanocubes (or cubooctahedra) of ~8 nm in dimension. When 0.5 mM $FeCl_3$ was added, the truncated nanocubes grew to a size of ~25 nm (Figure 1B). Addition of more $FeCl_3$ led to the formation of larger nanocubes. Figure 1C shows the TEM image of slightly truncated nanocubes of Pd with an average size of 50 nm, produced in the presence of 1.25 mM $FeCl_3$. The slightly truncated, cubic shape of large Pd nanoparticles is supported by high-resolution TEM studies (Figure 1D). The fringes in the HRTEM image are separated by 2.0 Å, which agrees with the {200} lattice spacing of face-centered cubic Pd. The fringe orientation in the HRTEM image implies that the nanoparticle is bound by six {100} facets and eight {111} facets. The ratio of {100} to {111} is relatively high, a

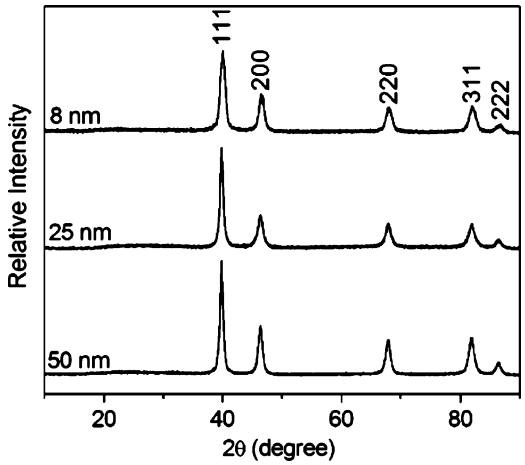

Figure 2. XRD patterns of Pd nanocubes with average sizes of 8, 25, and 50 nm.

distinctive characteristic of truncated cubes. The HRTEM image also confirms that the as-obtained particles are single crystals.

The XRD patterns of as-prepared Pd nanocubes with different sizes are shown in Figure 2. All of the peaks can be indexed to face-centered cubic Pd (Joint Committee on Powder Diffraction Standards (JCPDS) Card No. 05-0681, $a = 3.889$ Å). The peak width becomes narrower with increasing nanoparticle size. Through the use of the Scherrer formula on the (111) peak,[19] the ratio of the average nanoparticle sizes in the three samples is estimated as 1:3:6, respectively, which agrees with the TEM observations. In the case of Au and Ag nanocubes,[7c,14a,20] the {200} peaks in their XRD patterns were abnormally intense because the samples were exclusively comprised of nanocubes with sharp corners that were preferentially oriented with their {100} facets parallel to the supporting substrate. In the present case, because the truncated Pd nanocubes have larger corners and edges, they are more likely to lay at a random orientation on the supporting substrate. Thus, no significant change in the (200) peak intensity was observed in their diffraction patterns.

Undoubtedly, Fe^{III} played a critical role in the size control of Pd nanoparticles, as shown in the near linear relation between the $FeCl_3$ concentration and the cube size (Figure S1 of the Supporting Information). As calculated from the size of the product and the conversion of $[PdCl_4]^{2-}$ (Figure S2 of the Supporting Information), the seed density in the solution without any Fe^{III} is estimated as 8.9×10^{16} L^{-1}. With the addition of 0.5 mM $FeCl_3$, the seed density decreased to 2.8×10^{15} L^{-1}. When the concentration of $FeCl_3$ was further increased to 1.25 mM, the seed density dropped to 3.4×10^{14} L^{-1}. From these data, one can see that addition of Fe^{III} reduced the number of seeds greatly through oxidative etching. Because the concentration of Pd precursor was kept constant in all these syntheses, a decrease in the number of seeds led to the formation of larger nanoparticles as the final product.

The oxygen in air was also crucial to the size control, because it was responsible for the oxidation of Fe^{II} back to

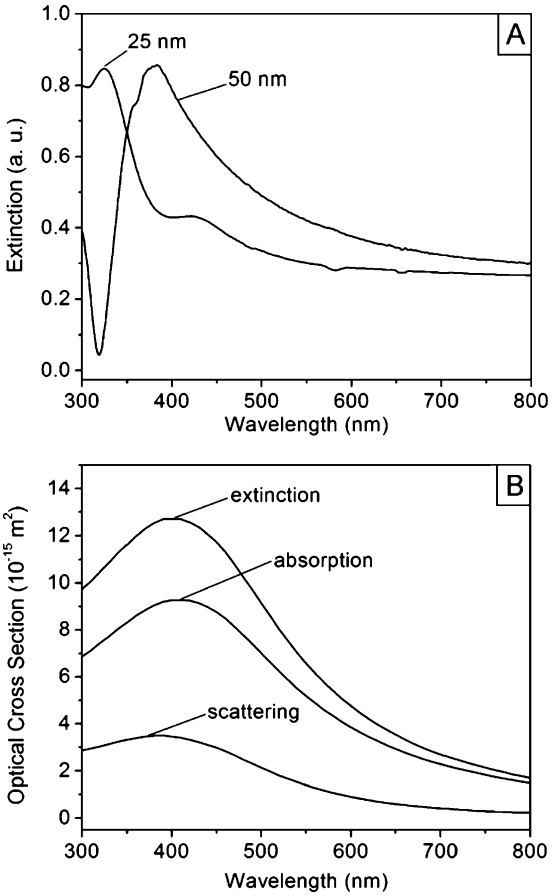

Figure 3. (A) UV−vis spectra of Pd nanocubes with average sizes of 25 and 50 nm. (B) Extinction, scattering, and absorption cross sections calculated for a Pd nanocube with an edge length of 50 nm using the DDA method.

Fe^{III}. At 90 °C, ethylene glycol could reduce Fe^{III} to Fe^{II}. Therefore, without oxygen, the concentration of Fe^{III} in the solution would quickly decrease. As Fe^{II} cannot oxidize Pd, seeds would not be etched. As shown in the Supporting Information (Figure S3 of the Supporting Information), if the reaction was performed with continuous bubbling of argon in the presence of 1.25 mM $FeCl_3$, then the nucleation density was reduced by Fe^{III} only within the first 2 min, after which nucleation accelerated. As a result, Pd nanoparticles of 10 nm in size eventually formed in the absence of air (Figure S4 of the Supporting Information).

The UV−vis extinction spectra of truncated Pd nanocubes indicate unique and size-dependent SPR properties. As calculated using the DDA method or Mie theory,[21] the resonance peak of Pd nanocubes of 8 nm in size is located at about 225 nm, beyond the spectral range from 300 to 1500 nm. The measured spectrum (Figure S5 of the Supporting Information) shows an extinction peak covering 200−240 nm. Note that the surfaces of as-prepared Pd nanocubes are usually covered by PVP, which has an absorption peak at 212 nm.[14b,15] Therefore, the observed extinction peak should be due to the convolution of the resonance peak of 8-nm Pd nanocubes and the absorption peak of PVP. However, the 25- and 50-nm nanocubes produced by this synthesis exhibit resonant peaks around 330 and 390 nm (Figure 3A), respectively. Figure 3B shows the extinction (C_{ext}), absorp-

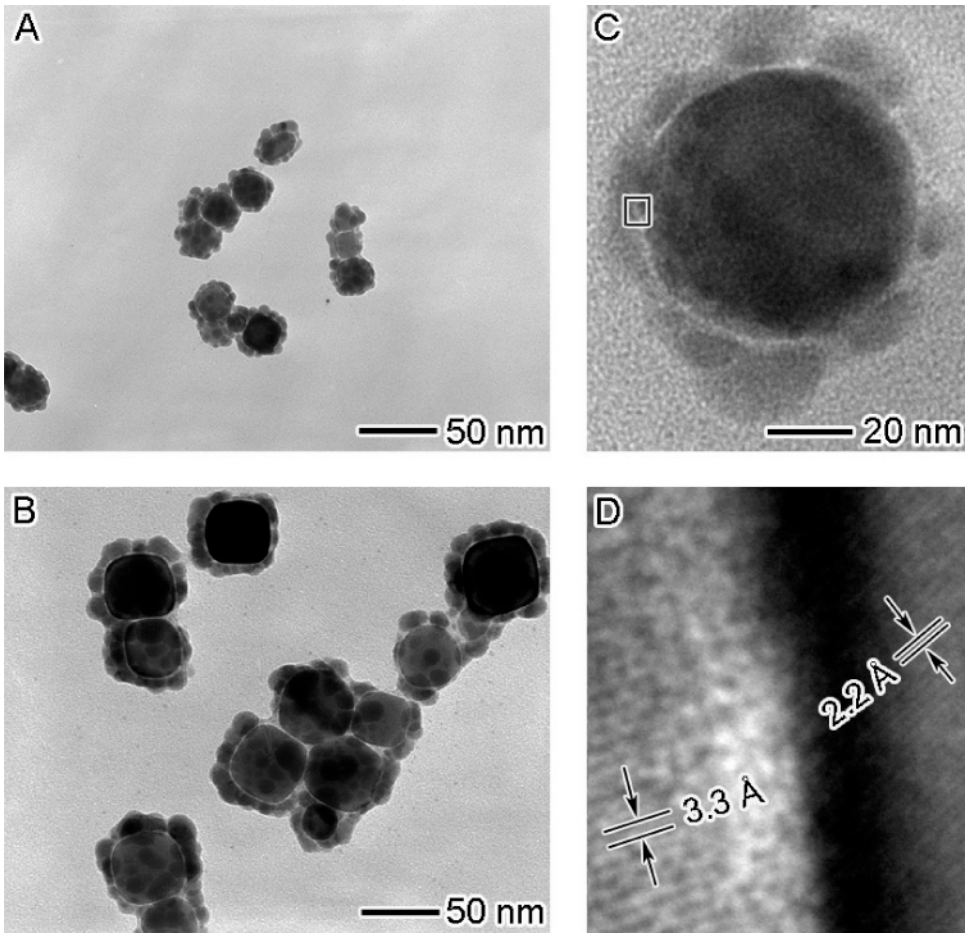

Figure 4. (A) TEM image of Pd nanocubes with an average size of 25 nm after exposure to air for 45 days. (B and C) TEM images of Pd nanocubes with an average size of 50 nm after exposure to air for 8 days. (D) HRTEM image taken from the portion labeled with a box in part C.

tion (C_{abs}), and scattering (C_{sca}) cross sections (note that $C_{ext} = C_{abs} + C_{sca}$) of a 50-nm Pd nanocube computed using the DDA method.[11] The location of the calculated peak matches well with the experimentally measured spectrum, but the real nanocubes seem to exhibit a sharper SPR peak than what is predicted. The polydispersity of synthesized nanoparticles usually results in wider SPR peaks than those predicted by DDA, making the narrowness of the Pd nanocube SPR peak an unusual feature that deserves further, systematic study. The shoulder peak at ~420 nm in the spectrum of ~25-nm nanocubes may be due to aggregation at this smaller size.

The stability of Pd nanocubes also exhibited size-dependence. A dried sample of 8-nm Pd nanocubes did not change shape when left in air over 90 days. In contrast, after being stored in air on TEM grids for about 45 days, 25-nm Pd nanocubes became core−shell-type particles with pores in the shell (Figure 4A). The 50-nm Pd nanocubes transformed into core−shell nanostructures (Figures 4B and 4C) after only 8 days. From HRTEM (Figure 4D), it was found that the shell was composed of discrete single-crystalline particles with an interplanar distance of 3.3 Å, while the core had an interplanar distance of 2.2 Å. The fringe distance of 3.3 Å could be indexed to the {111} planes of face-centered cubic PdO (JCPDS Card No. 46-1211, $a = 5.637$ Å), and the 2.2 Å corresponds to the {111} planes of Pd. Thus, the formation of a core−shell structure could be attributed to the oxidation of Pd by air. The formation of pores in the shell found in our case is an interesting feature associated with Pd oxidation. Suggested by the Cabrera−Mott theory[22] and experimental measurements,[23] the oxide formation is generally characterized by three distinct stages, (i) dissociative adsorption of oxygen on the surface, (ii) diffusion of oxygen atoms into the surface layer(s), and (iii) nucleation and formation of a surface oxide. In the process of oxide growth, the oxide could not "wet" the metal due to the large lattice mismatch between Pd and PdO. At the same time, individual oxide species are weekly bound to the Pd surface and can migrate to the growing PdO.[24] Hence, the oxide layers tend to form pores in the shell. Rather than to follow the principle that small particles have higher surface energy and are more active, the stability of Pd nanocubes *decreased* with the *increasing* size. This nonintuitive result may be related to the so-called "self-limiting oxidation" or "stress-limiting oxidation" effect.[25] The surfaces of Pd nanoparticles can readily be covered with thin conformal layers of oxide after exposure to air. For 8-nm nanocubes, because the oxide occupied a larger volume than the Pd, further oxidation would induce a stress at the Pd/PdO interface. When this stress accumulated to a certain amount, oxide formation would become energetically unfavorable.

This effect has been observed for the oxidation of Si nanowires with diameters less than 10 nm and covered by SiO_x thin layers.[25] Due to the stress (which is inversely proportional to the size of the particle), the thin layers of oxide on the surface of small Pd nanoparticles could protect them from further oxidation, resulting in excellent stability in air.

In summary, at the same concentration of Na_2PdCl_4 precursor, Pd nanocubes of 8, 25, and 50 nm were produced by controlling the number of initial seeds through addition of Fe^{III}. Because Fe^{III} could etch the Pd seeds, increasing the concentration of Fe^{III} resulted in the production of larger nanocubes. We believe that introduction of an oxidant into the synthesis of metal nanoparticles may provide a versatile tool to control their nucleation and growth into well-defined sizes and shapes. Excellent control of Pd nanocube size enabled an initial characterization of two unique size-dependent properties. First, although the Pd nanocubes below 10 nm have no SPR resonance above 300 nm, the 25- and 50-nm nanocubes displayed SPR peaks at 330 and 390 nm, respectively. The SPR properties of Pd nanostructures remain largely unexplored, but further tailoring of their size or shape may enable their SPR properties to be tuned in a way similar to silver and gold.[11,20,26] Second, 8-nm Pd nanocubes were stable in air for more than 90 days, but 50-nm nanocubes oxidized to generate Pd@PdO core−shell nanostructures in about 8 days. This oxidation phenomenon can likely be extended to fabricate metal oxide nanostructures with hollow interiors.

Acknowledgment. This work was supported in part by a DARPA-DURINT subcontract from Harvard University and a fellowship from the David and Lucile Packard Foundation. Y.X. is a Camille Dreyfus Teacher Scholar (2002). J.C. and B.W. thank the Center for Nanotechnology at the University of Washington for a Nanotech and an IGERT fellowship (funded by the National Science Foundation, Grant No. DGE-9987620), respectively. Z.-Y.L. was supported by the National Key Basic Research Special Foundation of China (Grant No. 2004CB719804). Y.Y. was supported by the Director, Office of Science, U.S. Department of Energy, under Contract No. DE-AC03-76SF00098. The authors thank the Molecular Foundry at the Lawrence Berkeley National Laboratory for HRTEM support. This work used the Nanotech User Facility, a member of the National Nanotechnology Infrastructure Network funded by the NSF.

Supporting Information Available: Dependence of cube dimension on the concentration of $FeCl_3$ added in the nucleation step, the concentration of $[PdCl_4]^{2-}$ remaining in reaction solutions after particle formation, photographs of a reaction performed in the presence of 1.25 mM $FeCl_3$ in air or under argon, TEM image of 10-nm Pd nanocubes obtained under argon in the presence of 1.25 mM $FeCl_3$, and UV−vis spectrum of Pd nanocubes with an average size of 8 nm as calculated using the DDA method. This material is available free of charge via the Internet at http://pubs.acs.org.

References

(1) Reviews: (a) Halperin, W. P. *Rev. Mod. Phys.* **1986**, *58*, 533. (b) Templeton, A. C.; Wuelfing, W. P.; Murray, R. W. *Acc. Chem. Res.* **2000**, *33*, 27.

(2) Catalysis and optics: (a) Lewis, L. N. *Chem. Rev.* **1993**, *93*, 2693. (b) Ahmadi, T. S.; Wang, Z. L.; Green, T. C.; Henglein, A.; El-Sayed, M. A. *Science* **1996**, *272*, 1924. (c) Murphy, C. J.; Jana, N. R. *Adv. Mater.* **2002**, *14*, 80. (d) Teng, X.; Black, D.; Watkins, N. J.; Gao, Y.; Yang, H. *Nano Lett.* **2003**, *3*, 261.

(3) Electronics and optoelectronics: (a) El-Sayed, M. A. *Acc. Chem. Res.* **2001**, *34*, 257. (b) Chen, S.; Yang, Y. *J. Am. Chem. Soc.* **2002**, *124*, 5280.

(4) Information storage: (a) Peyser, L. A.; Vinson, A. E.; Bartko, A. P.; Dickson, R. M. *Science* **2001**, *291*, 103. (b) Murray, C. B.; Sun, S.; Doyle, H.; Betley, T. *MRS Bull.* **2001**, *26*, 985.

(5) Sensing and clinical diagnostics: (a) Taton, T. A.; Mirkin, C. A.; Letsinger, R. L. *Science* **2000**, *289*, 1757. (b) Tkachenko, A. G.; Xie, H.; Coleman, D.; Glomm, W.; Ryan, J.; Anderson, M. F.; Franzen, S.; Feldheim, D. L. *J. Am. Chem. Soc.* **2003**, *125*, 4700. (c) Zhang, X.; Young, M. A.; Lyandres, O.; Van Duyne, R. P. *J. Am. Chem. Soc.* **2005**, *127*, 4484.

(6) SERS: (a) Nie, S.; Emory, S. R. *Science* **1997**, *275*, 1102. (b) Tessier, P. M.; Velev, O. D.; Kalambur, A. T.; Rabolt, J. F.; Lenhoff, A. M.; Kaler, E. W. *J. Am. Chem. Soc.* **2000**, *122*, 9554. (c) Cao, Y. C.; Jin, R.; Mirkin, C. A. *Science* **2002**, *297*, 1536. (d) Dick, L. A.; McFarland, A. D.; Haynes, C. L.; Van Duyne, R. P. *J. Phys. Chem. B* **2002**, *106*, 853.

(7) (a) Sun, S.; Murray, C. B.; Weller, D.; Folks, L.; Moser, A. *Science* **2000**, *287*, 1989. (b) Chen, S.; Wang, Z. L.; Ballato, J.; Foulger, S. H.; Carroll, D. L. *J. Am. Chem. Soc.* **2003**, *125*, 16186. (c) Caswell, K. K.; Wilson, J. N.; Bunz, U. H. F.; Murphy, C. J. *J. Am. Chem. Soc.* **2003**, *125*, 13914. (d) Jin, R.; Cao, Y. W.; Hao, E.; Metraux, G. S.; Schatz, G. C.; Mirkin, C. A. *Nature* **2003**, *425*, 487. (e) Kim, F.; Connor, S.; Song, H.; Kuykendall, T.; Yang, P. *Angew. Chem., Int. Ed.* **2004**, *43*, 3673. (f) Narayanan, R.; El-Sayed, M. A. *J. Phys. Chem. B* **2004**, *108*, 5726. (g) Hao, E.; Bailey, R. C.; Schatz, G. C.; Hupp, J. T.; Li, S. *Nano Lett.* **2004**, *4*, 327. (h) Yin, Y.; Rioux, R. M.; Erdonmez, C. K.; Hughes, S.; Somorjai, G. A.; Alivisatos, A. P. *Science* **2004**, *304*, 711.

(8) For example, see: (a) Fernández-García, M.; Martínez-Arias, A.; Salamanca, L. N.; Coronado, J. M.; Anderson, J. A.; Conesa, J. C.; Soria, J. *J. Catal.* **1999**, *187*, 474. (b) Nishihata, Y.; Mizuki, J.; Akao, T.; Tanaka, H.; Uenishi, M.; Kimura, M.; Okamoto, T.; Hamada, N. *Nature* **2002**, *418*, 164.

(9) For example, see: (a) Reetz, M. T.; Westermann, E. *Angew. Chem., Int. Ed.* **2000**, *39*, 165. (b) Franzén, R. *Can. J. Chem.* **2000**, *78*, 957. (c) Li, Y.; Hong, X. M.; Collard, D. M.; El-Sayed, M. A. *Org. Lett.* **2000**, *2*, 2385. (d) Kim, S.-W.; Kim, M.; Lee, W. Y.; Hyeon, T. *J. Am. Chem. Soc.* **2002**, *124*, 7642. (e) Son, S. U.; Jang, Y.; Park, J.; Na, H. B.; Park, H. M.; Yun, H. J.; Lee, J.; Hyeon, T. *J. Am. Chem. Soc.* **2004**, *126*, 5026.

(10) Tobiška, P.; Hugon, O.; Trouillet, A.; Gagnaire, H. *Sens. Actuators B* **2001**, *74*, 168.

(11) (a) Draine, B. T.; Flatau, P. J. *J. Opt. Soc. Am. A* **1994**, *11*, 1481. (b) Li, Z.-Y.; Gu, B. Y.; Yang, G. Z. *Phys. Rev. B* **1997**, *57*, 10883. (c) Jin, R.; Cao, Y.; Mirkin, C. A.; Kelly, K. L.; Schatz, G.; Zheng, J.-G. *Science* **2001**, *294*, 1901. (d) Sosa, I. O.; Noguez, C.; Barrera, R. G. *J. Phys. Chem. B* **2003**, *107*, 6269.

(12) (a) Teranishi, T.; Miyake, M. *Chem. Mater.* **1998**, *10*, 594. (b) Bradley, J. S.; Tesche, B.; Busser, W.; Maase, M.; Reetz, M. T. *J. Am. Chem. Soc.* **2000**, *122*, 4631. (c) Kim, S.-W.; Park, J.; Jang, Y.; Chung, Y.; Hwang, S.; Hyeon, T.; Kim, Y. W. *Nano Lett.* **2003**, *3*, 1289. (d) Veisz, B.; Király, Z. *Langmuir* **2003**, *19*, 4817. (e) Son, S. U.; Jang, Y.; Yoon, K. Y.; Kang, E.; Hyeon, T. *Nano Lett.* **2004**, *4*, 1147. (f) Gugliotti, L. A.; Feldheim, D. L.; Eaton, B. E. *Science* **2004**, *304*, 850.

(13) Fievet, F.; Lagier, J. P.; Figlarz, M. *MRS Bull.* **1989**, *14*, 29.

(14) (a) Sun, Y.; Xia, Y. *Science* **2002**, *298*, 2176. (b) Chen, J.; Herricks, T.; Geissler, M.; Xia, Y. *J. Am. Chem. Soc.* **2004**, *126*, 10854. (c) Wiley: B.; Herricks, T.; Sun, Y.; Xia, Y. *Nano Lett.* **2004**, *4*, 1733. (d) Wiley, B.; Sun, Y.; Mayers, B.; Xia, Y. *Chem.—Eur. J.* **2005**, *11*, 455.

(15) Xiong, Y.; Chen, J.; Wiley, B.; Xia, Y.; Aloni, S.; Yin, Y. *J. Am. Chem. Soc.* **2005**, *127*, 7332.

(16) Xia, Y.; Kim, E.; Whitesides, G. M. *J. Electrochem. Soc.* **1996**, *143*, 1070.

(17) In each synthesis, 5 mL of ethylene glycol (EG, J. T. Baker, 9300-01) was placed in a three-neck flask (equipped with a reflux condenser and a magnetic Teflon-coated stirring bar) and heated in air at 90 °C for 1 h. Meanwhile, 0.0162 g of palladium(II) sodium chloride (Na_2PdCl_4, Aldrich, 379808-1g) and 0.0312 g of poly(vinyl pyrrolidone) (PVP, Aldrich, 856568-100g, molecular weight = 55 000) were separately dissolved in 3 mL of EG at room temperature. These two solutions (with the molar ratio between Pd and the repeating unit of PVP being 1:5) were then injected simultaneously into the flask through a syringe pump at a rate of 45 mL per hour. Heating of the reaction at 90 °C was continued in air for 3 h. For iron-mediated synthesis, the other experimental parameters were kept the same except for the addition of $FeCl_3$ solution (in EG) before syringe pumping. The samples were washed with acetone and then with ethanol several times to remove most of the EG and PVP by centrifugation. The as-obtained samples were then characterized by transmission electron microscopy (TEM), high-resolution TEM (HRTEM), and powder X-ray diffraction (XRD). A drop of the aqueous suspension of particles was placed on a piece of carbon-coated copper grid (Ted Pella, Redding, CA) for TEM and dried under ambient conditions. The grid was then transferred to a gravity-fed flow cell and washed for 1 h with deionized water to remove the excess PVP. Finally, the sample was dried and stored in a vacuum for TEM characterization. TEM images were taken on a Phillips 420 transmission electron microscope operated at 120 kV. HRTEM images were taken on a JEOL 2010 LaB6 high-resolution transmission electron microscope operated at 200 kV. Powder XRD patterns were recorded on a Philips 1820 diffractometer equipped with a Cu Kα radiation source ($\lambda = 1.54180$ Å). UV−vis spectra were obtained using a Hewlett-Packard 8452A diode array spectrophotometer.

(18) *Handbook of Chemistry and Physics*, 60th ed.; Weast, R. C., Ed.; CRC Press: Boca Raton, FL, 1980.

(19) Klug, H. P.; Alexander, L. E. *X-Ray Diffraction Procedures for Polycrystalline and Amorphous Materials*; Wiley: New York, 1962; p 491.

(20) Im, S. H.; Lee, Y. T.; Wiley, B.; Xia, Y. *Angew. Chem., Int. Ed.* **2005**, *44*, 2154.

(21) Creighton, J. A.; Eadon, D. G. *J. Chem. Soc., Faraday Trans.* **1991**, *87*, 3881

(22) Ronay, M.; Latta, E. E. *Phys. Rev. B* **1985**, *32*, 5375.

(23) Voogt, E. H.; Mens, A. J. M.; Gijzeman, O. L. J.; Geus, J. W. *Surf. Sci.* **1997**, *373*, 210.

(24) (a) Giorgio, S.; Henry, C. R.; Chapon, C.; Roucau, C. *J. Catal.* **1994**, *148*, 534**.** (b) Rodriguez, N. M.; Oh, S. G.; Dalla-Betta, R. A.; Baker, R. T. K. *J. Catal.* **1995**, *157*, 676. (c) Bondzie, V. A.; Kleban, P. H.; Dwyer, D. J. *Surf. Sci.* **1996**, *347*, 319. (d) Bondzie, V. A.; Kleban, P. H.; Dwyer, D. J. *Surf. Sci.* **2000**, *465*, 266. (e) Stierle, A.; Kasper, N.; Dosch, H.; Lundgren, E.; Gustafson, J.; Mikkelsen, A.; Andersen, J. N. *J. Chem. Phys.* **2005**, *122*, 044706.

(25) (a) Liu, H.; Biegelsen, D. K.; Johnson, N. M.; Ponce, F. A.; Pease, R. F. W. *J. Vac. Sci. Technol., B* **1993**, *11*, 2532. (b) Liu, H.; Biegelsen, D. K.; Johnson, N. M.; Ponce, F. A.; Pease, R. F. W. *Appl. Phys. Lett.* **1994**, *64*, 1383. (c) Yin, Y.; Gates, B.; Xia, Y. *Adv. Mater.* **2000**, *12*, 1426.

(26) Jin, R. C.; Egusa, S.; Scherer, F. *J. Am. Chem. Soc.* **2004**, *126*, 9900.

NL0508826